Journal of Molecular Spectroscopy:

***Submitted** 22 February, 1997*

The ν_1 and ν_2 Bands of FNO_2

Charles E. Miller*[1] and Stanley P. Sander

Jet Propulsion Laboratory, California Institute of Technology

Mail Stop 183-901,4800 Oak Grove Drive, Pasadena, CA 91109-8099

[1]National Research Council/NASA Jet Propulsion Laboratory Research Associate

[2]Email: cmiller@ftuvs.jpl.nasa.gov

Number of Pages: 13

Number of Figures: 5

Number of Tables: 2

Proposed Running Head: The ν_1 and ν_2 Bands of FNO_2

Address correspondence to: Charles E. Miller

Jet Propulsion Laboratory

California Institute of Technology

Mail Stop 183-901,

4800 Oak Grove Drive,

Pasadena, CA 91109-8099

Email: cmiller@ftuvs.jpl.nasa.gov

Tel: 818,393.0228

FAX: 818.393.5019

ABSTRACT

High resolution infrared spectra of the strong a-type absorption corresponding to the ν_1 (ν_0 -1310.75 cm-l) and ν_2 (ν_0 = 821.9387 cm-l) bands of FNO_2 have been analyzed. The VI line positions exhibited extensive perturbations as a result of three nearly degenerate vibrational states - ν_1, $\nu_3+\nu_6$ and $\nu_5+\nu_6$ - which interact through strong Coriolis coupling. The weak Coriolis interaction between V_2 and ν_6 reported by Tanaka and Merino [*J. Mol. Spec/rose,* 32, 436-448 (1969)] manifested itself through changes in the b-axis constants of the V_2=1 state; nevertheless, over 1400 V_2 transitions were fit with an rrns error of 0.00066 cm-l using the standard A-reduced Hamiltonian. Line positions, assignments, and relative intensities for the dominant transitions in both bands have been established, although a comprehensive analysis of the perturbations requires a detailed understanding of the lower frequency vibrational states.

INTRODUCTION

There have been few previous spectroscopic studies of FNO_2 in excited vibrational states. Bernitt, Miller and Hisatsune obtained low resolution IR spectra of all six fundamentals and determined a harmonic force field (1). In two very interesting papers (2,3) Tanaka and Merino probed pure rotational transitions within the V_2, V_3, V_5, and ν_6 states using microwave spectroscopy.[†] They found that an extremely strong Coriolis interaction coupled the nearly degenerate V_3 and V_5 states, producing highly perturbed rotational energy levels in each state. Additionally, Tanaka and Merino noted that the rotational transition frequencies in the V_2 and ν_6 states deviated slightly from their calculated semirigid rotor values, They resolved these discrepancies by invoking an effective Hamiltonian based on a weak b-axis Coriolis coupling between V_2 and ν_6.

We obtained high resolution FTIR spectra of FNO_2 during an investigation of the product branching ratios in the F + NO_2 reaction (4). The strong ν_1 (-1310.7 cm-l), V_2 (-821.9 cm^{-1}) and ν_4 (-1793.4 cm-l) absorption were deemed excellent candidates for use in infrared kinetic monitoring of FNO_2; therefore, line positions, relative intensities, and assignments of the rotationally resolved spectra were required. In fact, Pagsberg et al. recently measured the F + NO_2 reaction rate constant using several FNO_2 rovibrational

[†] Note: the vibrational mode labeling convention used by Tanaka and Merino (3) differs from that used in the present study. The table below provides the correlations between the two sets of vibrational state designations.

	Mode Labeling Convention	
ν_0 / cm"'	This Work	Ref (3) Convention
1310.7	ν_1 (a_1)	ν_1 (a_1)
821.7	ν_2 (a_1)	ν_2 (a_1)
572.4	ν_3 (a_1)	ν_3 (a_1)
1793.4	ν_4 (b_1)	ν_5 (b_2)
562.5	ν_5 (b_1)	ν_6 (b_2)
741.8	ν_6 (b_2)	ν_4 (b_1)

from the ν_1 and ν_4 bands (5). This paper extends our analysis of the FNO_2 infrared spectrum to include the VI and V_2 bands; interpretation of the V_4 band has already been reported (6).

EXPERIMENTAL

The experimental method was identical to that reported previously (4,6). Spectra were recorded on a Bomem DA8-3 Fourier transform spectrometer optically coupled to a fast-flow/multipass absorption cell. Nitryl fluoride was produced by the reaction of fluorine atoms with NO_2

$$F + NO_2 \xrightarrow{M} FNO_2$$

A dedicated OMA (EG&G Princeton Applied Research) monitored the NO_2 and FNO_2 concentrations via absorption in the 200-360 nm range.

Spectra of the ν_1 band were recorded in transmission with a resolution of 0.004 cm-' and boxcar anodization using a 1230-1350 cm-l band pass filter (OCLI N0791 4); 128 scans were co-added to obtain the final spectrum. The NO_2 concentration in the reaction mixture was limited so that the strongest Q-branch features attenuated the transmission less than 50%. Spectra of the V_2 band were recorded with a resolution of 0.005 cm-l using a 730-1080 cm-l band pass filter (OCLI W1 1865). The reaction conditions were again controlled so that the strongest features attenuated the transmission less than 50'% and 128 scans were co-added to obtain the final spectrum. Infrared line positions were determined using the Bomem-Grams software package and assigned an experimental uncertainty of 0.001 cm^{-1}.

SPECTRAL ANALYSIS AND DISCUSSION

FNO_2 is an oblate rotor with C_{2v} symmetry. The presence of two indistinguishable ^{16}O nuclei requires that the molecular wavefunction follow Bose-Einstein statistics and that the rovibrational component of the wavefunction have even parity with respect to the molecular a-axis. The zero point vibrational state has al symmetry, as do the V_1= 1 and V_2= 1 states, therefore only rotational levels with even K_a values have non-zero spin-statistical weights in all three vibrational states. This results in purely a-type infrared spectra for both the VI and V_2 bands since all transitions must have ΔK_a = O, ±2, etc. The strong Q-branches typically associated with a-type bands are clearly seen in the overview spectra of VI (Figure 1) and V_2 (Figure 4).

Spectral calculations were performed using Pickett's SPINV program suite (7) and Watson's A-reduced Hamiltonian (8) in the III^l representation. Upper state constants were calculated relative to the ground state values and all constants were floated during the non-linear least squares fitting iterations. The 51 ground state microwave transitions reported in references (9), (10), and (11) were included in both the V_1 and V_2 line lists. The V_2 line list also included the nine microwave transitions measured for this state by Tanaka and Merino (2). Lines for which the (ohs-talc) residual was more than three times the experimental uncertainty of the line position were excluded from the fit.

1. The ν_1 spectrum

The $N0_2$ symmetric stretching motion gives rise to the strong ν_1 infrared absorption. Figure 1 shows that this band exhibits an intense, red-degraded Q-branch with an apparent bandhead at 1310,75 cm-l. The P- and R-branches contain a long series of well-resolved transition clusters with constant $2J''-K_c''$ values, as shown in Figure 2. The

rotational structure is similar to that observed in the V_4 band (6): P- and R-branch transitions occur in clusters regularly spaced at 0.42 cm-l intervals. The clusters contain a series of lines which converge toward the low wavenumber limit of each grouping. Beginning with the head of each cluster, the transitions originate from ground state vibrational levels with the quantum numbers $N_{0,N}$, N-1 $_{2,N-2}$, N-$2_{2,N-4}$, N-$3_{4,N-6}$, etc. where $N=2J''-K_c''$. The strongest line within each cluster has $K_c''=J''$ and the line strengths diminish as KC" decreases.

Figure 2 shows P-branch clusters for $2J''-K_c''$ values of 24, 23, and 22 beginning with the transitions $23_{0,23} \leftarrow 24._{,24}$ (1300.41" 39 cm-l), $22_{0,22} \leftarrow 23_{0,23}$ (1300.8459 cm-l), and 210,21 $\leftarrow$ 22.$_{,22}$ (1301.2778 cm-l), respectively. The spin-statistical weights of the ground and $v_1=1$ states ensure that only a-type transitions occur, as mentioned above. Since many transitions are "missing" from the spectrum, individual features are well spaced and easily resolved.

It was straightforward to assign individual rotational transitions within each $2J''-K_c''$ cluster using ground state combination differences. A line list covering the range $7< 2J''-K_c'' \leq 50$, $0 \leq K_a'' \leq$ 12 and containing more than 700 assignments was constructed in this fashion. However, the rrns IR residuals from the calculated v_1 line positions were on the order of 0.005 cm-l, or roughly an order of magnitude larger than expected. The line list was checked for misassignments using an interactive Loomis-Wood program (12): no gross errors were observed. Transition series with constant K_a'' could be fit to within the uncertainty anticipated for the data set (-0.0005 cm-l), but it remained impossible to fit all K_a'' series simultaneously with this precision. Very recently, Hegelund and coworkers

have observed similar behavior for fits to the ν_1 spectrum (13). Figure 3 shows the fitting residuals obtained for several fits to the $K_a'' = O$ transitions. Clearly, a significant perturbation affects this band,

Inspection of the lower frequency modes reveals two combination levels which should be virtually degenerate with VI: $\nu_3+\nu_6$ and $\nu_5+\nu_6$. We have observed the ν_3/ν_5 spectrum in the region near 570 cm-l and it exhibits extensive frequency and intensity perturbations. Tanaka and Merino observed microwave transitions for both of these states and noted a strong Coriolis interaction compounded by the near degeneracy of the V_3 and V_5 vibrational frequencies (2,3). The extensive mixing of the V_3 and ν_5 states suggests that the $\nu_3+\nu_6$ and $\nu_5+\nu_6$ combination levels are mixed to a similar extent, A successful fit of the V_1 spectrum is clearly predicated on a detailed understanding of the difficult ν_3/ν_5 problem and an analysis of the weak ν_6 fundamental.

2. The ν_2 spectrum

The spectrum observed in the 820 cm-* region is associated with the NO_2 bending vibration, V_2. This band displays a prominent blue-degraded Q-branch flanked by strong P- and R-branches, as shown in Figure 4. Figure 5 illustrates that the rotational structure in the V_2 band is more complicated than that of the VI band (Figure 2). The majority of strong rotational lines are still concentrated in $2J''-K_c''$ transition clusters, but these clusters now overlap. Additionally, the V_2 band contains numerous relatively strong transitions interspersed with the $2J''-K_c''$ clusters.

A preliminary calculation of the ν_2 spectrum was performed using the rotational and centrifugal distortion constants obtained from fitting the nine microwave transitions

reported by Tanaka and Merino (3); ν_0 was estimated from the Q-branch bandhead. A comparison between the experimental spectrum and this calculation showed that there were observed lines with the appropriate intensities and within 0.001 cm^{-1} of the calculated line positions for all $2J''-K_c'' \leq 15$ transitions, These lines were incorporated into the line list and a new prediction generated. Successive fitting iterations were used to expand the line list until more than 1300 P- and R-branch transitions had been assigned, Q-branch transitions were evaluated only after all P- and R-branch lines had been assigned. The density of intense lines in the 821.5-824 cm-l region made it impossible to assign every individual feature, but the addition of these transitions to the line list reduced the uncertainties in all of the V_2= 1 constants by approximately 15%. The final line list included 1432 infrared, 51 ground state microwave and nine V_2 microwave transitions spanning the quantum numbers $O \leq J' \leq 55, 0 \leq K_a' \leq 32, 0 < KC' \leq 55$ and the range 798-845 cm-l. The spectroscopic constants collected in Table 1 reproduced the infrared lines with an overall rrns error of 0.00066 cm-*.

We note that the final fitting iteration rejected five of the nine V_2 microwave transitions from the fit because the calculated line positions were more than 0.15 MHz (three times the experimental 0.05 MHz uncertainty) from the observed frequencies. A separate calculation performed with the experimental uncertainty increased from 0.05 to 0.10 MHz forced the fit to include all nine transitions; however, this increased the IR rms error by 4% and increased the V_2=1 parameter uncertainties by ~20%. The rms errors associated with the nine V_2 microwave transitions were 0.190 and 0.174 MHz when the experimental uncertainties were defined as 0.05 and 0.10 MHz, respectively. Tanaka and

Merino reported an rms error of 0.18 MHz for their final fit (2) which establishes an approximate minimum for calculations with an effective Hamiltonian (see below). Since forcing the fit to include all nine ν_2 microwave transitions results in a statistically significant decrease in the quality of the fitting parameters without a dramatic decrease in the residual rms error, the parameters reported in Table 1 are those determined using the 0.05 MHz uncertainty for the ν_2 microwave lines.

Table 1 compares the optimized spectroscopic constants determined from fitting the V_2 IR/microwave data set to those obtained by an appropriate transformation (14) of the Tanaka and Merino fit (3) to the V_2 microwave data, The rotational constants agree extremely well. The agreement among the centrifugal distortion constants is less favorable, The discrepancy is largest for the constants associated with the K projection of angular momentum, Δ_K, Δ_{JK} and δ_K, and most likely results from the fact that Tanaka and Merino only varied τ_{bbbb} from its ground state value while all of the centrifugal distortion constants were floated during fitting optimization in the present work. The V_2=1 centrifugal distortion constants display large changes relative to the corresponding ground state values, consistent with a perturbation affecting the V_2=1 rotational energy levels,

Tanaka and Merino argued that the V_2 and ν_6 states were coupled via a b-type Coriolis interaction based on their observed B_2 and B_6 rotational constants and the failure of rigid rotor calculations to reproduce the observed microwave line positions to within experimental error in both states (3). They assumed that the coupling was weak and could be treated through correction terms affecting only the b-axis centrifugal distortion constant. A value of $\tau_{bbbb} = -110.6$ kHz was obtained for this effective Hamiltonian; the

remaining V_2= 1 distortion constants were constrained to the ground state values.

We have converted our A-reduced Hamiltonian centrifugal distortion constants into distortion constants for the reduced Hamiltonian and collected these in Table 2 along with the Tanaka and Merino distortion constants. The agreement between the τ_{bbbb} values is remarkably good. In fact, all of the distortion constants agree to within 10°/0 except for τ_{aabb} where there is a factor of 2.5 difference between the Tanaka and Merino value and that of the present work. This suggests that the a-axis and b-axis motions in V_2 are not completely decoupled, although this is a good first order approximation, We conclude that the spectroscopic constants presented in Table 1 are those of an effective Hamiltonian and that do not reflect the unperturbed values of the V_2=1 state despite the excellent precision of the calculated line positions. The ability of this effective Hamiltonian to reproduce the experimental observations so accurately suggests that the Coriolis coupling problem will be readily solved with a simultaneous fit of the V_2 and ν_6 spectra, Such an analysis is under investigation by Hegelund (15).

CONCLUSIONS

We have analyzed high resolution infrared spectra of the ν_1 and ν_2 bands of FNO_2. Both bands exhibited upper state perturbations associated with Coriolis interactions. In the case of ν_1, these interactions are thought to be due to the presence of two dark states, $\nu_3+\nu_6$ and $\nu_5+\nu_6$, which are nearly degenerate with ν_1. Because of the perturbations in the upper state, transitions which were easily assigned using ground state combination differences defied accurate fitting with a standard A-reduced Hamiltonian. It was possible to obtain excellent fits for V_2 spectrum with a standard A-reduced

Hamiltonian. The resulting constants must be treated as fitting parameters, however, since they represent the optimization of an effective Hamiltonian. The determination of deperturbed spectroscopic constants for both ν_1 and ν_2 will be possible once the analysis of the lower frequency vibrational bands has been completed.

ACKNOWLEDGMENTS

The authors would like to thank E. A. Cohen for helpful discussions and P. Pagsberg and F. Hegelund for communicating their results prior to publication, This work was performed at the Jet Propulsion Laboratory, California Institute of Technology, under contract with the National Aeronautics and Space Administration.

REFERENCES

1. D. L. Bernitt, R. H. Miller, and I. C. Hisatsune, *Spectrochim. Acts 23A, 237-248 (1967).*

2, T. Tanaka and Y. Merino, *J. Mol. Spectrosc. 32, 430-435(1969).*

3. T. Tanaka and Y. Merino, *J. Mol. Spectrosc. 32,436-448 (1969).*

4, C. E. Miller and S. P. Sander, submitted to *J. Phys. Chem.*

5. P. Pagsberg, A. Sillesen, J. T. Jodkowski, and E. Ratajczak, *Chem. Phys. Lett.* 252, 165-171 (1996).

6. C. E. Miller and S. P. Sander, to appear in *J. Mol. Spectrosc. 181,* No. 1 (1997).

7. H. M. Pickett, *J. Mol. Spectrosc. 148,371-377 (1991).*

8. J. K. G. Watson, J. *Chem. Phys. 48,4517-4528 (1968).*

9. A. C. Legon and D. J. Millen, *J. Chem. Sot. A* 1968, 1736-1740 (1968).

10. A.M. Mirri, G. Cazzoli, and L. Ferretti, *J. Chem. Phys. 49,2775-2780 (1968).*

11, C. Styger, B. Gatehouse, N. Heineking, W. Jäger, and M. C. L. Gerry, *J. Chem. Sot. Faraday Trans. 89,* 1899-1902 (1993).

12. B. P. Winnewisser, J, Reinstädtler, K. M. T. Yamada, and J. Behrend, *J.* Mol. *Spec/rose.* 136, 12-16 (1989); F. Stroh, *Thesis,* Justus-Liebig Universität Giessen (1991).

13. F. Hegelund, P. Pagsberg, H. Burger, and G. Pawelke, poster J38, The 14th International Conference on High Resolution Molecular Spectroscopy, Prague, Czech Republic, September 9-13, 1996.

14. W. Gordy and R. L, Cook, *Microwave Molecular Spectra,* Chapter 8, Wiley Interscience/New York, 1984.

15. F. Hegelund, private communication (1996).

FIGURE CAPTIONS

Figure 1, An overview of the ν_1 spectrum.

Figure 2, An expanded view of several $2J''-K_c''=N$ clusters in the ν_1 P-branch. The feature marked A is associated with a transition between levels with high KC values, See text for details.

Figure 3. Fitting residuals for the $K_a'' = O$ series in ν_1. Circles: residuals from a fourth order polynomial fit to the $K_a'' = O$ lines only, Squares: residuals for the $K_a'' = O$ series obtained from the A-reduced Hamiltonian fit to all assigned ν_1 lines.

Figure 4. An overview of the ν_2 spectrum.

Figure 5. An expanded view of several $2J''-K_c''=N$ clusters in the ν_2 P-branch. Upper panel: simulation; lower panel: experimental spectrum. Compare to Figure 2.

TABLE 1

Fitting Parameters for the FNO_2 Ground and ν_2=1 States[a,b]

Parameter	Ground State	ν_2	ν_2=1	V_2=1 (Ref. 3)[c]
A/MHz	13201,34908 (234)		13207.4315	13207.35
(A'-A")/MHz		*6.0824 (76)*		
B/MHz	11446.20034 (144)		11546.0705	11546.07
(B'-B")/MHz		99.8702 (75)		
C/MHz	6119.00100 (105)		6104.8050	6104.74
(C'-C")/MHz		-14.1960(51)		
Δ_J/kHz	14.8350(161)		18.853	18.802
(Δ_J'- Δ_J")/kHz		4.018 (53)		
Δ_{JK}/kHz	-16.986 (65)		-32.235	-26.763
(Δ_{JK}'- Δ_{JK}")/kHz		-15.249 (103)		
Δ_K/kHz	3.817 (52)		14.987	10.205
(Δ_K'- Δ_K")/kHz		11.170(210)		
δ_J/kHz	2.3936 (67)		3,7593	4.424
(δ_J'- δ_J")/kHz		1,3657 (270)		
δ_K/kHz	-23.341 (135)		-9.65	-11.031
(δ_K'- δ_K")/kHz		13.69 (22)		
ν_0/cm^{-1}		821.938735 (70)		
rms error/cm-l		0.00066		

[a]Numbers in parentheses after each constant reflect the 1σ error in units of the last digit.

[b]Constants determined from the data set consisting of 58 MW, 2 FTMW and 1430 IR transitions using Watson's A-reduced Hamiltonian and the III^l representation.

[c]Quartic centrifugal distortion constants calculated from the $\tau_{\alpha\beta\gamma\delta}$ values reported in Reference 3, see Table 2,

Table 2

Distortion Constants for the ν_2 Band Expressed

in Terms of the Reduced **Hamiltonian**[a]

	This work	Tanaka and Merino (Ref. 3)
τ_{aaaa}	-45.338	-39.814
τ_{bbbb}	-105.486	-110.6
τ_{aabb}	32.595	12.452
τ_{abab}	-54,470	-48.868

'All values given in kHz.

LIST OF SYMBOLS

Symbol	Definition
A, B, C	Principal rotational constants
A“, B“, C“	Principal rotational constants for the lower state in a specified transition
A’, B’, C’	Principal rotational constants for the upper state in a specified transition
Δ_K, A_J, A_{JK}, δ_J, δ_K	Quartic centrifugal distortion constants in the A-reduction
$\tau_{\alpha\beta\gamma\delta}$	Distortion constant for the anular momentum operator $P_\alpha P_\beta P_\gamma P_\delta$
τ_{aaaa}, τ_{bbbb}, τ_{aabb}, τ_{abab}	Axis specific quartic centrifugal distortion constants
ν_0	Origin of a vibrational transition

Journal of Molecular Spectroscopy, C.E. Miller and S.P. Sander, Figure 1

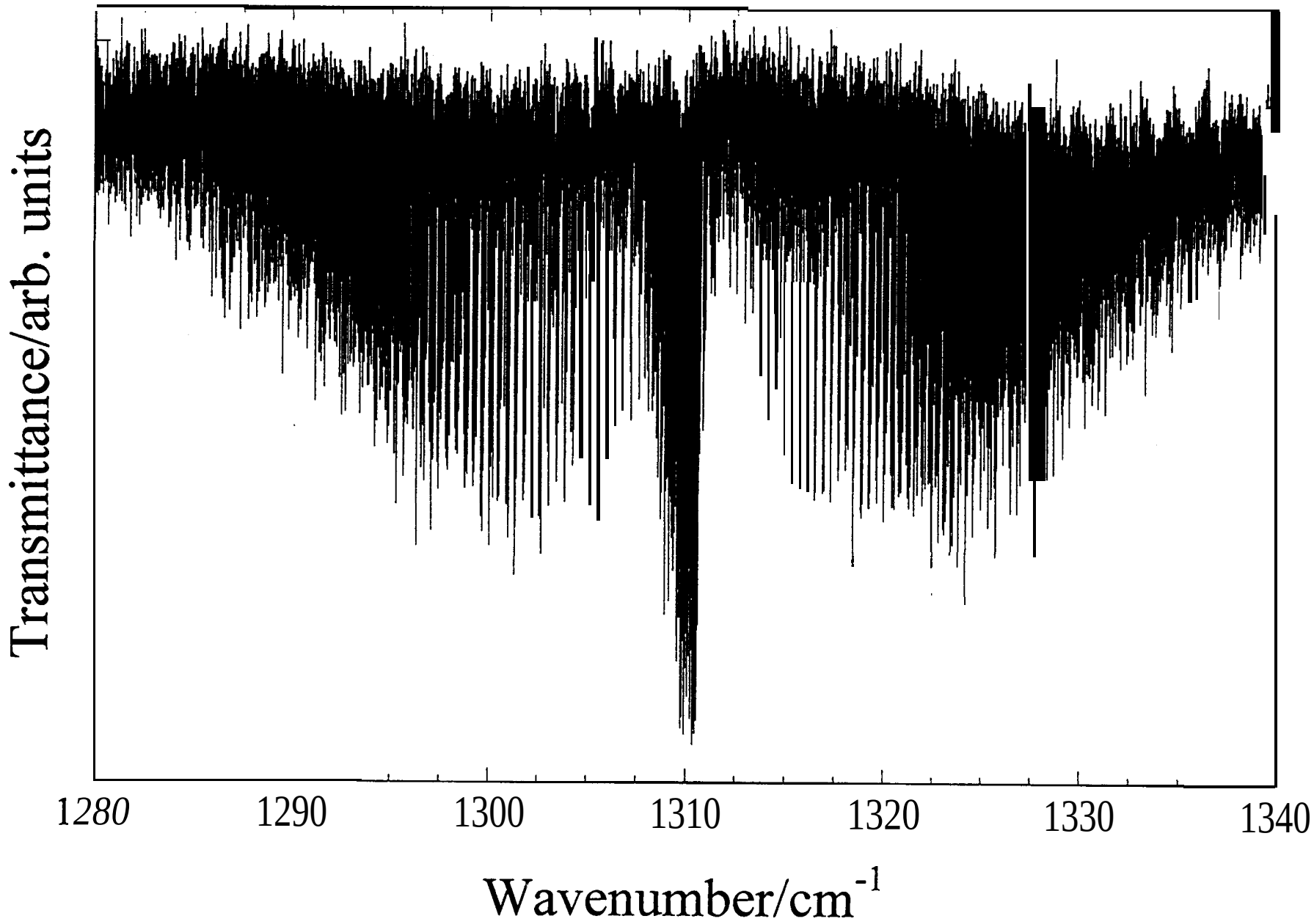

Journal of Molecular Spectroscopy, C.E. Miller and S.P. Sander, Figure 2

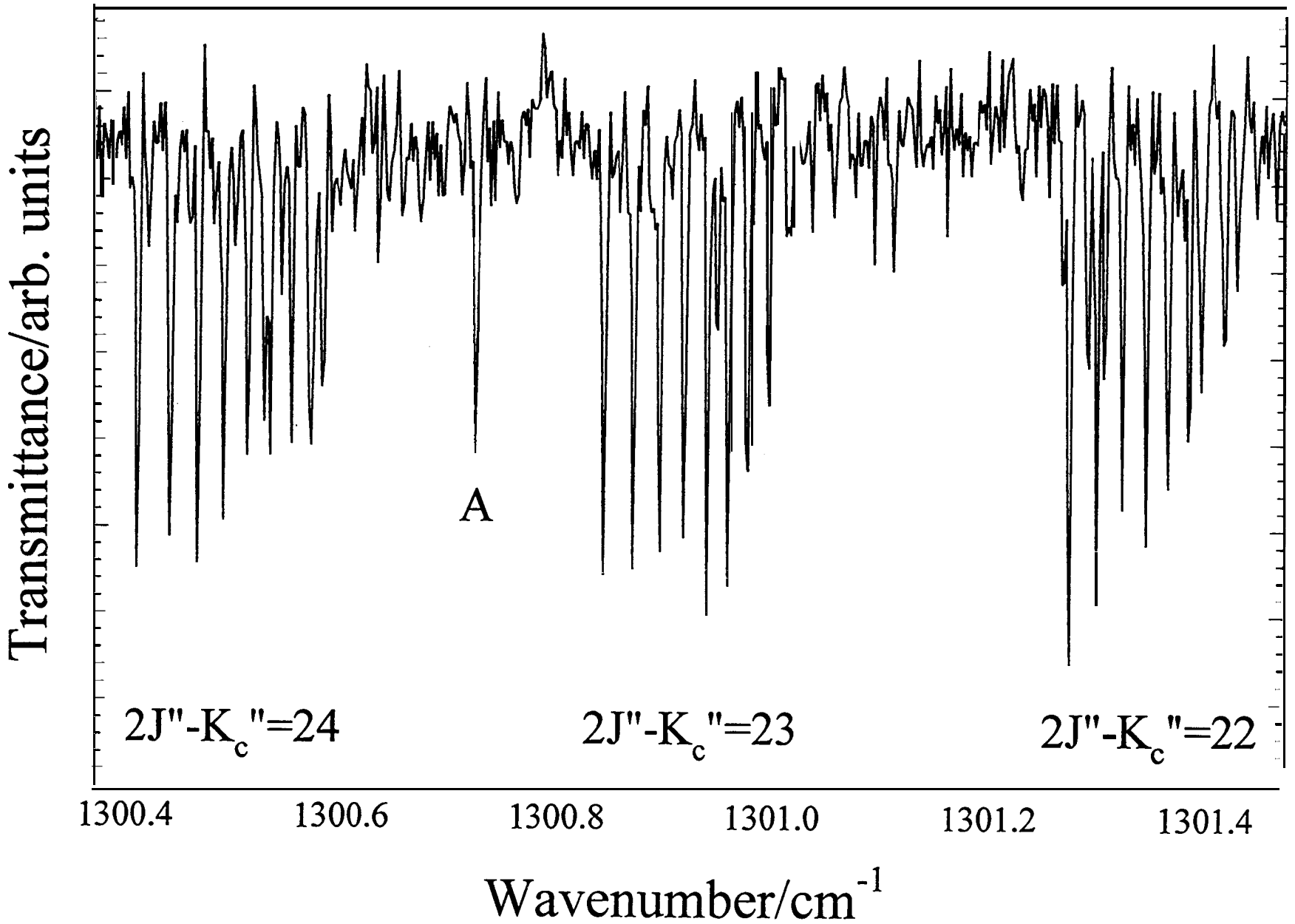

Journal of Molecular Spectroscopy, C.E. Miller and S.P. Sander, Figure 3

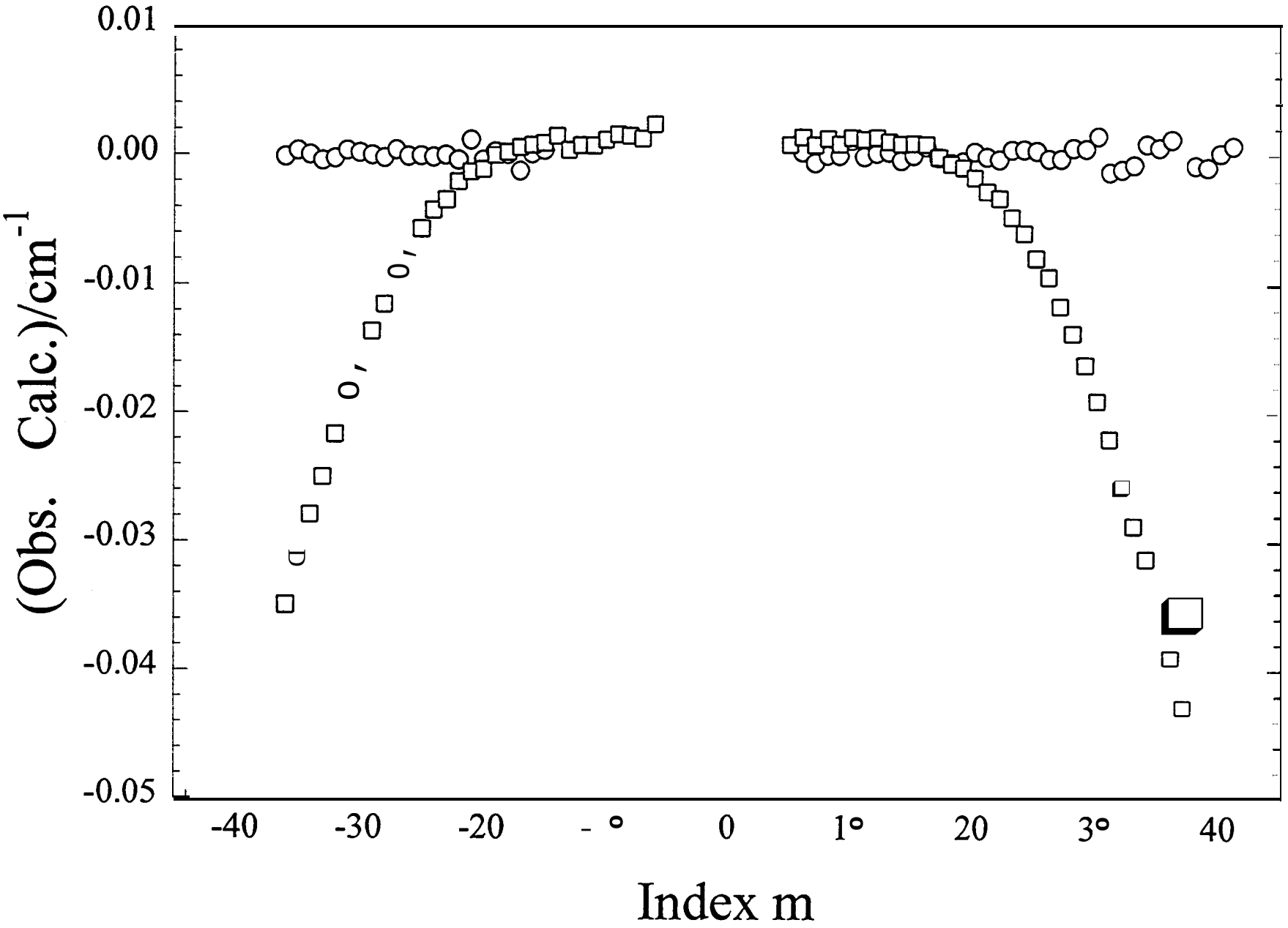

Journal of Molecular Spectroscopy, C.E. Miller and S.P. Sander, Figure 4

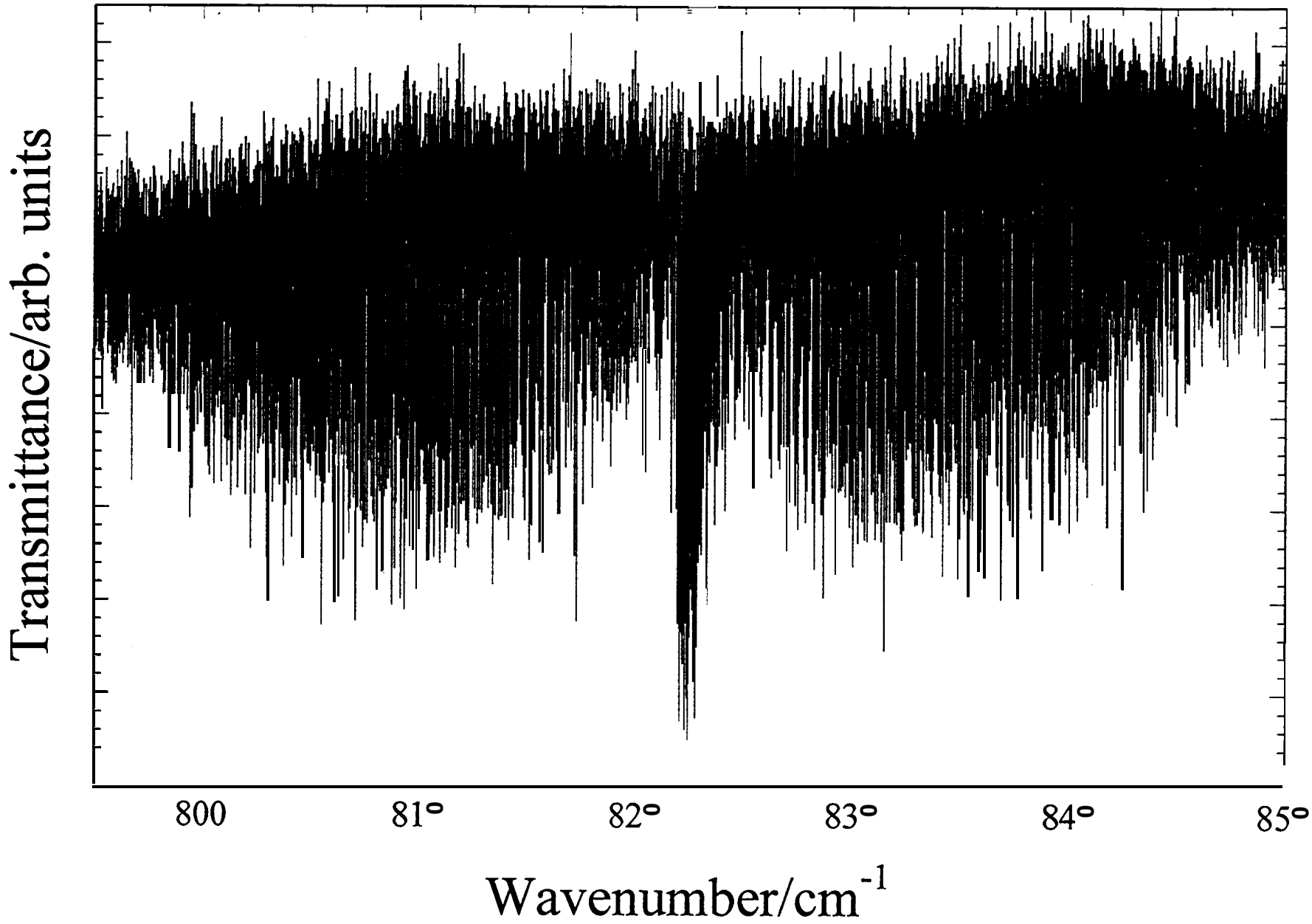

Journal of Molecular Spectroscopy, C.E. Miller and S.P. Sander, Figure 5